Effect of anode polarization on biofilm formation and electron transfer in Shewanella oneidensis /graphite felt microbial fuel cells

David Pinto, T. Coradin, Christel Laberty-Robert

Effect of Anode Polarization on Biofilm Formation and Electron Transfer in *Shewanella oneidensis*/Graphite Felt Microbial Fuel Cells

David Pinto [a], *Thibaud Coradin* [a], *Christel Laberty-Robert* [a]*

[a] Sorbonne Universités, UPMC Univ. Paris 06, CNRS-UMR 7574, Collège de France, Laboratoire de Chimie de la Matière Condensée de Paris, 4 place Jussieu, 75005 Paris, France

KEYWORDS. Microbial Fuel Cell, *Shewanella oneidensis*, biofilm, bacteria/carbon interface, polarization.

ABSTRACT. In microbial fuel cell, electricity generation is assumed by bacterial degradation of low-grade organics generating electrons that are transfered to an electrode. The nature and efficiency of the electron transfer from the bacteria to the electrodes are determined by several chemical, physical and biological parameters. In particular, the application of a specific potential at the bioanode has been shown to stimulate the formation of an electro-active biofilm but the underlying mechanisms remain poorly understood. In this context, we have here studied the effect of an applied potential on the formation and electroactivity of biofilms established by *Shewanella oneidensis* bacteria on graphite felt electrodes in single- and double-chamber reactor configurations, in oxic conditions. Using amperometry, cyclic voltammetry and OCP/Power/Polarization curves techniques, we showed that a potential ranging between - 0.3 V and + 0.5 V (vs. Ag/AgCl/KCl sat.) and oppositely applied to a couple of electrodes leads to different electrochemical behaviors, anodic currents and biofilm architectures. In particular, when the bacteria were confined in the anodic compartment of a double-chamber cell, a negative applied potential (- 0.3 V) at the bioanode favors a mediated electron transfer correlated with the progressive formation of a biofilm filling the felt porosity and bridging the graphite fibers. In contrast, a positive applied potential (+ 0.3 V) at the bioanode stimulates a direct electron transfer resulting in the fast-bacterial colonization of the fibers only. These

results provide fruitful insights for the understanding of the complex bacteria-electrode interplay in microbial fuel cells.

INTRODUCTION

Microbial fuel cell (MFC) represents a promising energetical solution allowing the production of electricity from a diversity of organic substrates through direct oxidation by electrochemical active microorganisms under ambient conditions [1]. The power density output of an MFC is far lower than that of chemical fuel cell because the latter uses relatively clean energy sources such as hydrogen or methanol without implying other biological system, while MFCs typically use low-grade organics, such as domestic or industrial wastes. However, in return, using MFCs for waste treatment may significantly save energy [2].

Many parameters influence the performance of MFCs. Besides the electrode materials and the used micro-organisms, there is accumulating evidence that the potential applied at the bioanode impacts on its colonization and therefore the MFC electrochemical performance [3–8]. However the intensity and the sign of the potential is often a matter of discussion [9,10] and highly dependent on the micro-organisms which can be a bacterium or a consortium artificially-build or sampled from real environment [4,11], such as domestic or industrial wastewaters [12], garden composts [13] or marine soils [14]. As an example, for *Geobacter sulfurreducens* positive applied potential (ca. + 0.26 V vs. SCE, between 0 to + 0.4 V vs. Ag/AgCl [15] or + 0.51 V vs Ag/AgCl [16] depending on the quoted study) was necessary. For mixed cultures and real inoculum, the behavior is often more complex, due to the multiplicity of bacterium strains, the synergic behavior of these strains and/or the domination of a specific strain. Moreover, the origin of inoculum influences its composition, and therefore its electrochemical response [17].

Most of the time, the potential is empirically defined and, to date, no general law exists to predict the “ideal potential of polarization” with efficiency and accuracy. However, the use of a potential higher than the standard potential of the electron donor that is degraded is necessary [18]. Note that potential higher than the equilibrium potential favors electron deficiency at electrode surface, then encouraging oxidation reaction by bacteria [19]. In most cases, the polarization as well as the measurements are carried out in strict anoxic condition [20,21] to limit the competition with oxygen reaction for electron collection and to ensure the viability of anoxic strains such as *G. sulfurreducens*.

In this context, the aim of the present work is to study whether the potential applied at a bioelectrode constituted of *S. oneidensis* bacteria in contact with a graphite felt (GF) in oxic conditions affects or not the MFC performances. Two different MFC configurations were employed, single- and dual-chamber MFC configuration [21,22], in order to apply opposite polarization at the two graphite felt electrodes considered as a bioanode [23] and a cathode [24–27]. The applied potential was varied from - 0.3 V to + 0.5 V (vs. Ag/AgCl/KCl sat.) at the bioanode and its influence on biofilm formation and MFC electrochemical performances was studied. Electrochemical activity was measured by monitoring electrodes open-circuit potential, current density, MFC open-circuit voltage, and MFC polarization curves (maximal current and power) [28]. Moreover, the characterization of the biofilm organization after several days of functioning permitted to establish correlations between the electrochemical response and the colonization progress that was found to be sensitive to the sign and intensity of the applied potential.

MATERIALS AND METHODS

All chemicals are bioreagent grad, provided by Sigma-Aldrich France and used without further purification. The graphite felt is gratefully delivered by Morgan Carbon company (Luxembourg) [29]. *S. oneidensis* CRBIP17.141 bacterial strain is prepared and delivered by Biological Resource Center of the Pasteur Institute (France).

Inoculum. *S. oneidensis* inoculum is prepared following two steps of pre-growth and growth. A fraction of the strain, conserved at -80°C, is inoculated and pre-cultivated into a Luria-Bertani Broth medium stirred at 150 rpm for 24 h at 30°C. Then, 1 mL of the pre-cultivated bacteria is transferred into a 50 mL MR1 growth-medium (see SI for complete description) with 30 mM sodium lactate and sodium fumarate as electron donor (carbon source) and electron acceptor, respectively. Bacterial growth is carried out for 18 h in oxic condition until reaching an optical density (at 600 nm, OD_{600}) corresponding to the last quarter of the log-phase (OD_{600} = 1.7) of the bacterial growth. The final inoculum is prepared by transferring the obtained bacterial pellet into fresh MR1 medium supplemented with 30 mM sodium lactate and free of sodium fumarate. The inoculum is stored at 4 °C in

sterile oxic condition for 10 min before being used as electrolyte for electrochemical reactor.

Single- and dual-chamber reactor set-up and polarization experiment. In both single- and dual-chamber reactors, GF was used as anode (1 cm^3) and cathode (2 cm^3, to ensure no current limitation due to the cathodic electro-active surface). A three electrodes configuration was employed for electrodes polarization and for electrochemical characterization using Ag/AgCl/KCl sat. reference electrode.

The single-chamber configuration was composed of a 30 mL sealed vessel. The GF anode and cathode were used in 20 mL of the *S. oneidensis* inoculum diluted at 0.7 in OD_{600}, corresponding to 8 10^8 $cfu.mL^{-1}$. For all experiment, *S. oneidensis* inoculum corresponds to the reactor electrolyte composed of bacteria dispersed in a MR1 medium (growth medium, as previously described) supplemented with 30 mM lactate and free from fumarate, buffered at pH 7.

For the dual-chamber configuration, two compartments were separated by an ultrafiltration membrane (pore size: 0.2 µm). The anodic side was filled with a bacteria solution (as previously described) and the catholyte consisted in a solution of 10 mM $K_3Fe(CN)_6$ and 150 mM NaCl. Both GF anode and cathode were placed at 2.5 cm from the separator together with an Ag/AgCl/KCl sat. reference in each compartment (figure S1, Supplementary Information). Lactate was supplemented in the anodic compartment and interval between additions of 30 mM lactate was evaluated by current monitoring; decreasing of current corresponds to a decrease in lactate availability. To ensure sterility, all the reactors components were autoclaved at 120 °C and then assembled in sterile conditions. The oxic condition was achieved during the whole experiment with vent-caps and sterile filters (pore size: 0.2 µm) to ensure atmospheric exchange.

To apply fixed potential at electrodes, the anode and the cathode were symmetrically and continuously polarized by applying well-defined potentials against a reference electrode (figure S1, Supplementary Information). The polarization effect was evaluated for anodic potential varying between - 0.3 V and + 0.5 V (vs. Ag/AgCl/KCl sat.) while the potential at the cathode was oppositely poised. Both the polarization step and the electrochemical characterizations were carried out in oxic condition.

Electrochemical and Scanning electron microscopic characterization. The evolution of the bio-anodic electrode was electrochemically monitored by chronoamperometry at + 0.3 V vs. Ag/AgCl/KCl sat. (after stabilization of the measured current, *ca*. 1 h) and cyclic-voltammetry (scan rate: 10 $mV.s^{-1}$). All the electrochemical characterizations were carried out with a Biologic VSP potentiostat in a 3-electrodes configuration with an Ag/AgCl/KCl saturated (sat.) reference electrode (figure S1, Supplementary Information). Anodic and cathodic open-circuit potential (OCP) were also monitored. In the dual-chamber configuration, polarization and power curves were determined by monitoring anodic and cathodic potential for an incremental series of current *i*, corresponding to equivalent defined densities of current *j* (mA per square centimeter of geometric surface area). Before electrochemical characterization, electrodes were left for stabilization at the OCP for 1 h.

After several days of polarization, anode and cathode materials were characterized by scanning electron microscopy (Hitachi S-3400N). To prevent degradation of the biological structures at the surface of the GF fibers, the samples were chemically fixed by their immersion in several successive baths. First, the sample was immersed in a 2.5 % glutaraldehyde and 0.1 M sodium cacodylate solution for 2 h at 4 °C and then washed three times in a bath of 0.2 M cacodylate for 10 min each. Finally, the sample was dehydrated in several baths of ethanol from 30 % to 100 % and dry in air.

RESULTS AND DISCUSSION

Single compartment studies. A first set of reference experiments was performed in single-chamber reactor in the absence of polarization using a freshly-prepared highly-concentrated suspension of *S. oneidensis* in PBS supplemented with 30 mM sodium lactate, in oxic conditions and using a platinum electrode as working electrode (at t_0 when bacteria were transferred in PBS). Cyclovoltamograms showed two sigmoidal waves of oxidation demonstrating the existence of two distinct mechanisms of electron transfer. According to the literature [9], they correspond to MET (Mediated Electron Transfer) for potentials below 0 V vs. Ag/AgCl/KCl sat. and DET (Direct Electron Transfer) for potentials above 0 V vs. Ag/AgCl/KCl sat. (Figure 1).

HERE FIGURE 1

In a second set of experiments, *S. oneidensis* bacteria harvested in the log phase and resuspended in MR1 medium containing 30 mM lactate were used and the anodic and cathodic applied voltage at the carbon felt electrodes were varied from - 0.3 V to + 0.5 V vs. Ag/AgCl/KCl sat. (Ec = - Ea).

Chronoamperometry experiments were performed over 19 days (Figure 2). In the presence of a negative polarization, the current was 60 μA after 1 day, dropped down to less than 10 μA after 4 days and then continued to decrease despite the regular lactate feeding. In the absence of polarization, the initial current was smaller (*ca.* 35 μA) and also underwent a rapid decrease but then increased again until it reached *ca.* 20 μA after 19 days. When a +0.3 V vs. Ag/AgCl/KCl sat. polarization was applied, the initial decrease phase was also observed and the current values varied around 50 μA average value. Finally, for a + 0.5 V vs. Ag/AgCl/KCl sat. potential, the current was stable over the first days of the experiment and then increases progressively to reach *ca.* 120 μA. Nevertheless, we observed a reproducible dispersion of current values at a given time points, suggesting that such high potentials may impact the bacterial activity and/or the stability of the bacteria-electrode interface.

HERE FIGURE 2

Cyclovoltamograms were recorded at different times of the experiments (Figure 3). After one day, regardless of the applied potential, cyclovoltamograms exhibited a pair of reversible faradaic peaks centered at - 0.4 V vs. Ag/AgCl/KCl sat. corresponding to riboflavin. An endogenous oxidation wave of similar shape and intensity was observed in the high positive and negative potential regions (Figure 3a) responsible for an extracellular electron transfer. After 4 days, the oxidation wave has increased in intensity for a + 0.5 V vs. Ag/AgCl/KCl sat. and a + 0.3 V vs. Ag/AgCl/KCl sat. polarization, in agreement with the chronoamperometry measurements (Figure 3b). In parallel, in the negative potential range, the signal becomes more complex, with an apparent splitting of the riboflavin peak. Such a splitting is confirmed at day 8 for all polarization conditions (Figure 3c). In parallel,

the oxidative wave has gained in intensity for systems under a positive polarization and especially at + 0.5 V vs. Ag/AgCl/KCl sat.. These two observations are still valid at day 19 although, for a + 0.5 V vs. Ag/AgCl/KCl sat. polarization, the two peaks appear to have merged (Figure 3d), resulting in a single signal in the same potential region but much broader than at day 1 (Figure 3a).

HERE FIGURE 3

These sets of experiments confirm the existence of different electron transfer mechanism (DET and/or MET/riboflavin), depending on the applied potential. On the one hand, the continuous increase in the intensity of the signal in the positive potential range suggests that the DET mechanism becomes more and more effective with time, especially under highly positive polarization conditions. This should reflect that an increasing number of bacteria are in direct contact with the graphite felt electrodes (*i.e.* anode colonization) and/or that the electron transfer at the bacteria/electrode interface becomes facilitated. For a non-polarized electrode or a polarization at -0.3 V vs. Ag/AgCl/KCl sat. the increasing of the wave intensity is less marked. On the other hand, the signals in the negative potential range do not evolve much in intensity but rather in shape. This can indicate the production of other mediators by the bacteria and/or a modification of the mediator/graphite interface. In particular, the splitting of the riboflavin peak may correspond to the co-existence of molecules originating from bacteria in solution and within the deposited biofilm.

To clarify these points, SEM imaging of the samples were performed at the end of the chronoamperometry experiments (Figure 4). The lowest density of bacteria is observed at a negative potential (Ea = - 0.3 V vs. Ag/AgCl/KCl sat.). These bacteria are embedded in a dense biofilm. Under non-polarized condition or positive applied potential, a similar situation is observed but the cell density seems higher, although biological analyses would be necessary to quantitatively ascertain this point. While the specific case of negative polarization fits well with the measurement of a very low current value, it is clear that the biofilm morphology, as it is observed here, cannot explain the differences in the electrochemical behavior for the other polarization conditions. Hence, the applied potential should have a deep impact on the internal structure and organization of the biofilm,

influencing the diffusion of the mediator and/or the connectivity of the conductive elements.

HERE FIGURE 4

Double compartment studies. In a step forward the development of a complete MFC, a dual compartment reactor was set up using an ultrafiltration membrane (pore size = 0.2 µm) as a separator to prevent bacterial diffusion from the anodic side to the cathodic compartment. A potential of either + 0.3 V or - 0.3 V was applied at the GF anode with an oppositely polarized cathode. The electrochemical behavior under symmetrical polarization was monitored by chronoamperometry and the evolution of the anode potential, polarization and the power curves as function of time were established

Figure 5 displays the evolution of the polarization and power curves over 19 days using a symmetrical polarization when the anode was polarized at + 0.3 V vs. Ag/AgCl/KCl sat. (vs. Ec = - 0.3 V vs. Ag/AgCl/KCl sat.). At day 2, the potential of the bioanode is equal to - 0.4 V vs. Ag/AgCl/KCl sat. and remains stable until the end of the experiment (Figure 5a). The anodic current density at Ea = 0 V vs. Ag/AgCl/KCl sat. evolves from 70 (day 2) to 30 $mA.m^{-2}$ (day 19). The evolution of the MFC polarization curves (Figure 5b) is a result of the anodic and cathodic *I-V* profiles. MFC OCV remains stable at *ca.* 0.65 V, indicating that the electroactivity established at the bioanode is stable. The internal resistance (polarization curve slope, $R_{INT} = \Delta E/j$) increases with time. Since no detrimental clogging of the separator was observed after 19 days, such an increase indicates a modification of electron transfer at the surface of the bioanode. This is confirmed by evolution of the current density (the maximum current density decreases from *ca.* 100 to 35 $mA.m^{-2}$) and the power curves (Figure 5c) where a loss in power from *ca.* 20 (day 2) to *ca.* 7 $mW.m^{-2}$ (day 19) was observed.

HERE FIGURE 5

The same experiment was performed with a - 0.3 V vs. Ag/AgCl/KCl sat. negative potential applied to the bioanode. Figure 6 summarizes the evolution of the characteristic

polarization and power curves. At the open-circuit, the potential of the bioanode (figure 6a) regularly decreases from - 0.25 V (day 2) to - 0.6 V vs. Ag/AgCl/KCl sat. (day 15). The MFC OCV shown in figure 6b increases from 0.5 V (day 2) to 0.85 V (day 15). Additionally, the maximal power density increases from 12 to 20 $mW.m^{-2}$ (figure 6c). The initial maximal density of current is about 100 $mA.m^{-2}$ and decreases to 60 $mA.m^{-2}$ at day 5 and then increases again to *ca.* 70 $mA.m^{-2}$ (17% recovered) and remains stable until day 15. Noticeably, a loss of electrochemical performances was observed after 19 days that can be explained by the depletion in lactate due to the absence of feeding after day 13.

HERE FIGURE 6

These results indicate two different behaviors as function of the polarization condition applied. Figure 7 summarizes the different situations: for both negative (- 0.3 V) and positive (+ 0.3 V) polarization, the maximal MFC current decreases in the first 5 days from 100 to about 60 $mA.m^{-2}$. Then, the value remains stable or slowly decreases. For an applied potential of + 0.3 V vs. Ag/AgCl/KCl sat., the MFC OCV remains constant at + 0.65 V while the power density decreases with time from *ca.* 20 $mW.m^{-2}$ to 5 $mW.m^{-2}$. This can be linked to a modification of the electron transfer from bacteria to graphite electrodes, correlated with the increase of the ohmic losses of the MFC. On the contrary, for applied potential of - 0.3 V vs. Ag/AgCl/KCl sat., an increase of the MFC OCV, from 0.55 V to 0.85 V, and power density, from 12 $mW.m^{-2}$ to 20 $mW.m^{-2}$, are observed, keeping day 19 data aside. The progressive increase of MFC OCV suggests a longer phase of stabilization for the bacteria in contact with the graphite anode compared to the positive applied potential. Additionally, the increase in power density can be linked to a better transfer of electron from the bacteria to the GF fibers.

HERE FIGURE 7

The microstructure of the electrode after 19 days was studied by scanning electron microscopy (figure 8). For a potential applied at the bioanode of + 0.3 V vs. Ag/AgCl/KCl

sat., the bacteria can be distinctly observed at the surface of fibers and form a uniform layer. This bacterial layer is embedded in a thin and dense biofilm which forms a sheath wrapped around the fibers. In contrast, for potential applied at the bioanode of - 0.3 V vs. Ag/AgCl/KCl sat., a large quantity of biomass (EPS, bacteria, …) occupies the porosity formed by the graphite fiber network. The fibers themselves are embedded in a thick and porous biofilm structure composed of a high density of bacteria and EPS.

HERE FIGURE 8

These observations can be related to the results of the single compartment experiments. Under positive polarization, DET becomes rapidly prevalent over MET, which can be correlated with an efficient colonization of the fiber surface by bacteria. In these conditions, as the biofilm thickens, the electron transfer may become less favorable, leading to a decrease in the electrochemical performance as observed for MFC power density. Yet, the MFC OCV remains stable meaning that the efficiency of the redox reaction and electron transfer at the fiber surface remains the same. In contrast, under negative polarization, both DET and MET are involved in the electron transfer, so that bacteria growth is favored both in solution, *i.e.* in the felt porosity, and on the fiber surface. In these conditions, the increase in the power density with time can be related to the simultaneous development of both populations. Moreover, the ability of the biofilm to bridge graphite fibers may provide additional conduction pathways. Yet it is interesting to point out that such bridging structures were not observed in single compartment experiments. This difference can be explained considering that, in the latter situation, the cathode is also in contact with the bacterial suspension and can interfere with its behavior. As a matter of fact, in these conditions, colonization of the graphite felt used as the counter-electrode could be observed by SEM (figure S3, Supplementary Information). On the contrary, in the double compartment configuration, the oppositely polarized electrode is isolated from the bacterial anolyte by the ultrafiltration membrane so that bacterial behavior must be influenced only by the anodic potential of polarization.

CONCLUSION

In this work, the impact of polarization on the colonization of graphite felts used as bioanodes by wild type *S. oneidensis* in oxic conditions and its influence on the electrochemical performances of single- and double-compartment fuel cells were studied. In single-compartment MFC configurations, both anodic current and electrode colonization are directly correlated to positive polarization (+ 0.3 and + 0.5 V vs. Ag/AgCl/KCl sat.). Under non-polarized condition, a lower and less reproducible current is measured but it remains higher than the current measured under negative polarization. These results suggest that positive polarizations favor the felt colonization but also impact the properties of the resulting biofilm. However, we also observed an unintended colonization of the counter electrode, which suggests a combined effect of both fixed anode and cathode potentials. To elucidate this phenomenon and prevent the cathode colonization by bacteria, dual-compartments MFC experiments were carried out in the same polarization conditions. Two distinct behaviors are observed: (i) under positive polarization, MFC performance (polarization and power curves), anodic OCP and MFC OCV are already at their maximal value after a short time of polarization; however, MFC performances decrease rapidly with time. The biofilm appears thin and dense around the felt fibers. (ii) Under negative polarization, the electrochemical parameters progressively increase to reach their maximal values after more than 20 days. In this condition, the biofilm is thick, porous and fills the porosity of the felt. These two behaviors seem in agreement with the DET/MET hypothesis. At + 0.3 V vs. Ag/AgCl/KCl sat., the electrode colonization is controlled by DET leading to the accumulation of bacteria on the fiber surface. On the contrary, at - 0.3 V vs. Ag/AgCl/KCl sat., the MET mechanism is more effective, driving the development of bacteria in the liquid phase, *i.e.* colonization of the felt porosity. Yet, biofilm formation of the fiber surface is also observed, suggesting that DET can also occur. Whether a negative potential favor MET, hinder DET or both remains an open question.

AUTHOR INFORMATION

Corresponding Author

*** Christel Laberty-Robert**

Sorbonne Universités, UPMC Univ. Paris 06, CNRS-UMR 7574

Laboratoire de Chimie de la Matière Condensée de Paris

Boite 174

4, place Jussieu

75005 Paris

@: christel.laberty@upmc.fr

ACKNOWLEDGMENT.

Authors gratefully thank the Direction Générale de l'Armement (DGA) for its funding. This work was supported by the Direction Générale de l'Armement - Mission pour la Recherche et l'Innovation Scientifique (DGA-MRIS).

ABBREVIATIONS

GF: graphite felt, Ea: anodic potential, Ec: cathodic potential, OD_{600}: Optical Density at 600 nm, MFC: microbial fuel cell, OCV: open-circuit voltage, OCP: open-circuit potential, SEM: scanning electron microscopy, $cfu.mL^{-1}$: colony-forming unit per milliliter, I-V curve: current-tension curve.

REFERENCES

(1) Pant, D.; Van Bogaert, G.; Diels, L.; Vanbroekhoven, K. A Review of the Substrates Used in Microbial Fuel Cells (MFCs) for Sustainable Energy Production. *Bioresour. Technol.* **2010**, *101* (6), 1533.

(2) Zhou, M.; Chi, M.; Wang, H.; Jin, T. Anode Modification by Electrochemical Oxidation: A New Practical Method to Improve the Performance of Microbial Fuel Cells. *Biochem. Eng. J.* **2012**, *60*, 151.

(3) Lewis, K. Symposium on Bioelectrochemistry of Microorganisms, IV. Biochemical Fuel Cells. *Bacteriol. Rev.* **1966**, *30* (1), 101.

(4) Rabaey, K.; Verstraete, W. Microbial Fuel Cells: Novel Biotechnology for Energy Generation. *Trends Biotechnol.* **2005**, *23* (6), 291.

(5) Wingard, L. B.; Shaw, C. H.; Castner, J. F. Bioelectrochemical Fuel Cells. *Enzyme and Microbial Technology*. 1982, pp 137–142.

(6) Bullen, R. A.; Arnot, T. C.; Lakeman, J. B.; Walsh, F. C. Biofuel Cells and Their Development. *Biosens. Bioelectron.* **2006**, *21*, 2015.

(7) Aghababaie, M.; Farhadian, M.; Jeihanipour, A.; Biria, D. Effective Factors on the Performance of Microbial Fuel Cells in Wastewater Treatment – a Review. *Environ. Technol. Rev.* **2015**, *2515* (October), 1.

(8) Ieropoulos, I. A.; Ledezma, P.; Stinchcombe, A.; Papaharalabos, G.; Melhuish, C.; Greenman, J. Waste to Real Energy: The First MFC Powered Mobile Phone. *Phys. Chem. Chem. Phys.* **2013**, *15* (37), 15312.

(9) Roy, J. N.; Babanova, S.; Garcia, K. E.; Cornejo, J.; Ista, L. K.; Atanassov, P. Catalytic Biofilm Formation by Shewanella Oneidensis MR-1 and Anode Characterization by Expanded Uncertainty. *Electrochim. Acta* **2013**.

(10) Jorge, A. B.; Hazael, R. Use of *Shewanella Oneidensis* for Energy Conversion in Microbial Fuel Cells. *Macromol. Chem. Phys.* **2016**, 1.

(11) Logan, B. E. Exoelectrogenic Bacteria That Power Microbial Fuel Cells. *Nat. Rev. Microbiol.* **2009**, *7* (5), 375.

(12) Sun, J.; Hu, Y.; Bi, Z.; Cao, Y. Improved Performance of Air-Cathode Single-Chamber Microbial Fuel Cell for Wastewater Treatment Using Microfiltration Membranes and Multiple Sludge Inoculation. *J. Power Sources* **2009**, *187* (2), 471.

(13) Cercado, B.; Byrne, N.; Bertrand, M.; Pocaznoi, D.; Rimboud, M.; Achouak, W.; Bergel, A. Garden Compost Inoculum Leads to Microbial Bioanodes with Potential-

Independent Characteristics. *Bioresour. Technol.* **2013**, *134*, 276.

(14) Lowy, D. A.; Tender, L. M.; Zeikus, J. G.; Park, D. H.; Lovley, D. R. Harvesting Energy from the Marine Sediment-Water Interface II. Kinetic Activity of Anode Materials. *Biosens. Bioelectron.* **2006**, *21* (11), 2058.

(15) Wei, J.; Liang, P.; Cao, X.; Huang, X. A New Insight into Potential Regulation on Growth and Power Generation of Geobacter Sulfurreducens in Microbial Fuel Cells Based on Energy Viewpoint. *Environ. Sci. Technol.* **2010**, *44* (8), 3187.

(16) Dumas, C.; Basseguy, R.; Bergel, A. Electrochemical Activity of Geobacter Sulfurreducens Biofilms on Stainless Steel Anodes. *Electrochim. Acta* **2008**, *53* (16), 5235.

(17) Roy, J. N.; Garcia, K. E.; Luckarift, H. R.; Falase, A.; Cornejo, J.; Babanova, S.; Schuler, a. J.; Johnson, G. R.; Atanassov, P. B. Applied Electrode Potential Leads to Shewanella Oneidensis MR-1 Biofilms Engaged in Direct Electron Transfer. *J. Electrochem. Soc.* **2013**, *160* (11), H866.

(18) Babauta, J.; Renslow, R.; Lewandowski, Z.; Beyenal, H. Electrochemically Active Biofilms: Facts and Fiction. A Review. *Biofouling* **2012**, *28* (8), 789.

(19) Bard, A. J.; Faulkner, L. R.; York, N.; Bullet, C.; Brisbane, W.; Toronto, S. E. *Electrochemical Methods: Fundamentals and Applications*; 1944.

(20) Wagner, R. C.; Call, D. F.; Logan, B. E. Optimal Set Anode Potentials Vary in Bioelectrochemical Systems. *Environ. Sci. Technol.* **2010**, *44* (16), 6036.

(21) Kumar, A.; Katuri, K.; Lens, P.; Leech, D. Does Bioelectrochemical Cell Configuration and Anode Potential Affect Biofilm Response? *Biochem. Soc. Trans.* **2012**, *40* (6), 1308.

(22) Liu, H.; Cheng, S.; Logan, B. E. Power Generation in Fed-Batch Microbial Fuel Cells as a Function of Ionic Strength, Temperature, and Reactor Configuration. *Environ. Sci. Technol.* **2005**, *39* (14), 5488.

(23) Gregory, K. B.; Bond, D. R.; Lovley, D. R. Graphite Electrodes as Electron Donors for Anaerobic Respiration. *Environ. Microbiol.* **2004**, *6* (6), 596.

(24) Bond, D. R.; Strycharz-Glaven, S. M.; Tender, L. M.; Torres, C. I. On Electron Transport through Geobacter Biofilms. *ChemSusChem* **2012**, *5* (6), 1099.

(25) Suzanne T Read, Paritam Dutta, Phillip L Bond, Jürg Keller, K. R. Initial Development and Structure of Biofilms on Microbial Fuel Cell Anodes. *BMC Microbiol.* **2010**, *10* (1), 98 (1.

(26) Gorby, Y.; McLean, J.; Korenevsky, a; Rosso, K.; El-Naggar, M. Y.; Beveridge, T. J. Redox-Reactive Membrane Vesicles Produced by Shewanella. *Geobiology* **2008**, *6* (3), 232.

(27) El-Naggar, M. Y.; Wanger, G.; Leung, K. M.; Yuzvinsky, T. D.; Southam, G.; Yang, J.; Lau, W. M.; Nealson, K. H.; Gorby, Y. a. Electrical Transport along Bacterial Nanowires from Shewanella Oneidensis MR-1. *Proc. Natl. Acad. Sci. U. S. A.* **2010**, *107* (42), 18127.

(28) Logan, B. E.; Hamelers, B.; Rozendal, R.; Schröder, U.; Keller, J.; Freguia, S.; Aelterman, P.; Verstraete, W.; Rabaey, K. Microbial Fuel Cells: Methodology and Technology. *Environ. Sci. Technol.* **2006**, *40* (17), 5181.

(29) Le Ouay, B.; Coradin, T.; Laberty-Robert, C. Mass Transport Properties of Silicified Graphite Felt Electrodes. *J. Phys. Chem. C* **2013**, *117* (31), 15918.

FIGURES CAPTIONS

Figure 1. Cyclic voltammetry at 10 $mV.s^{-1}$ of a highly concentrated suspension of S. oneidensis in a PBS buffer supplemented with 30 mM lactate in oxic conditions. The potential range corresponding to mediated electron transfer (MET, red zone) and direct electron transfer (DET, blue zone) and the corresponding scheme are adapted from Roy *et al.* [9].

Figure 2. Chronoamperometry measurements for *S. oneidensis*/graphite felt bioanodes in single-compartement reactors with an applied potential of (orange circles and squares) - 0.3 V, (blue circles and squares) 0 V, (green circles and squares) + 0.3 V and (dark circles and squares) + 0.5 V

Figure 3. Cyclovoltammograms at 10 $mV.s^{-1}$ for *S. oneidensis*/graphite felt bioanodes in single-compartement reactors with an applied potential of (orange line) – 0.3 V, (blue line) 0 V, (green line) + 0.3 V and (dark lines) + 0.5 V after (a) 1 day, (b) 4 days, (c) 8 days and (d) 19 days of polarization. Reference signal of GF/MR1 without bacteria and reference signal of riboflavin on figure S2 (Supplementary Information).

Figure 4. SEM observations of *S. oneidensis*/graphite felt bioanodes in single-compartement reactors. Representative morphology of colonized felts (a) and higher magnification images for bioanodes polarized at (b) + 0.5 V, (c) + 0.3 V, (d) non polarized, (e) - 0.3 V, after 19 days in working condition.

Figure 5. Electrochemical characterization of *S. oneidensis*/graphite felt// $K_3Fe(CN)_6$/graphite felt double-compartment reactor with a bioanode polarized at + 0.3 V after (orange circle) 2 days, (grey circle) 5 days, (green circle) 6 days, (blue circle) 15 days and (dark circle) 19 days: (a) anodic I-V, (b) polarization and (c) power curves.

Figure 6. Electrochemical characterization of *S. oneidensis*/graphite felt// $K_3Fe(CN)_6$/graphite felt double-compartment reactor with a bioanode polarized at - 0.3 V after (orange circle) 2 days, (grey circle) 5 days, (green circle) 6 days, (blue circle) 15 days and (dark circle) 19 days: (a) anodic I-V, (b) polarization and (c) power curves.

Figure 7. Temporal evolution of (dark circle) open-circuit voltage (OCV), (red circle) maximal power density and (blue circle) maximal current density for a *S. oneidensis*/graphite felt//$K_3Fe(CN)_6$/graphite felt double-compartment reactor with a bioanode polarized at (a) + 0.3 V and (b) -0.3 V.

Figure 8. SEM images of the anodic graphite felt interior after 19 days of function for a *S. oneidensis*/graphite felt//$K_3Fe(CN)_6$/graphite felt double-compartment reactor with a bioanode polarized at (a) + 0.3 V and (b) -0.3 V.

FIGURES

FIGURE 1

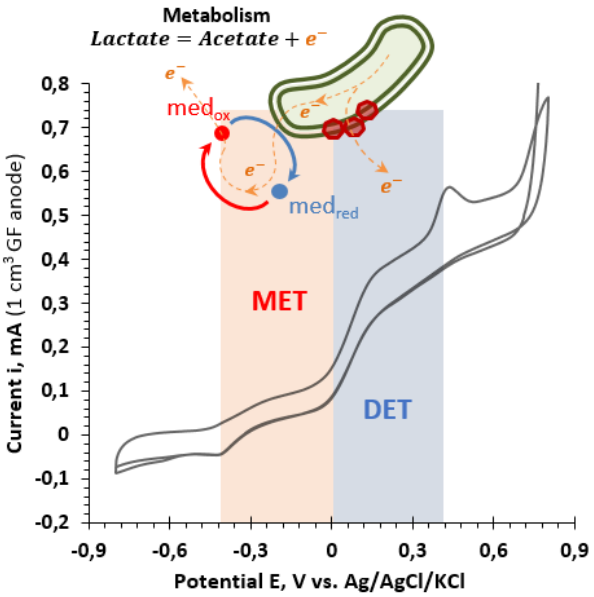

FIGURE 2

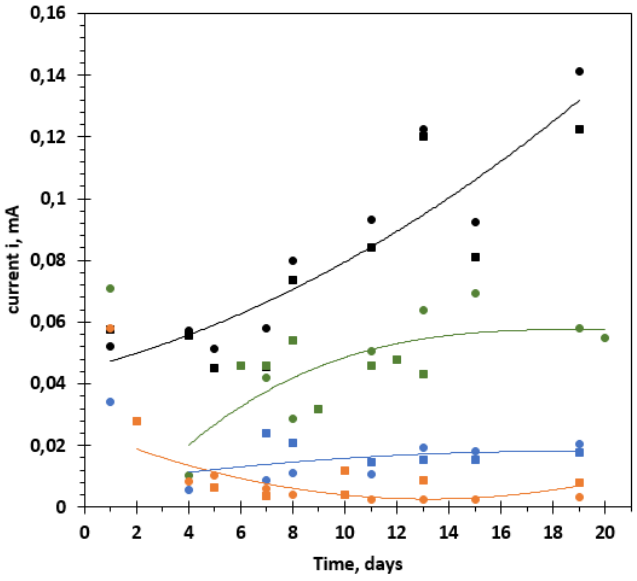

FIGURE 3

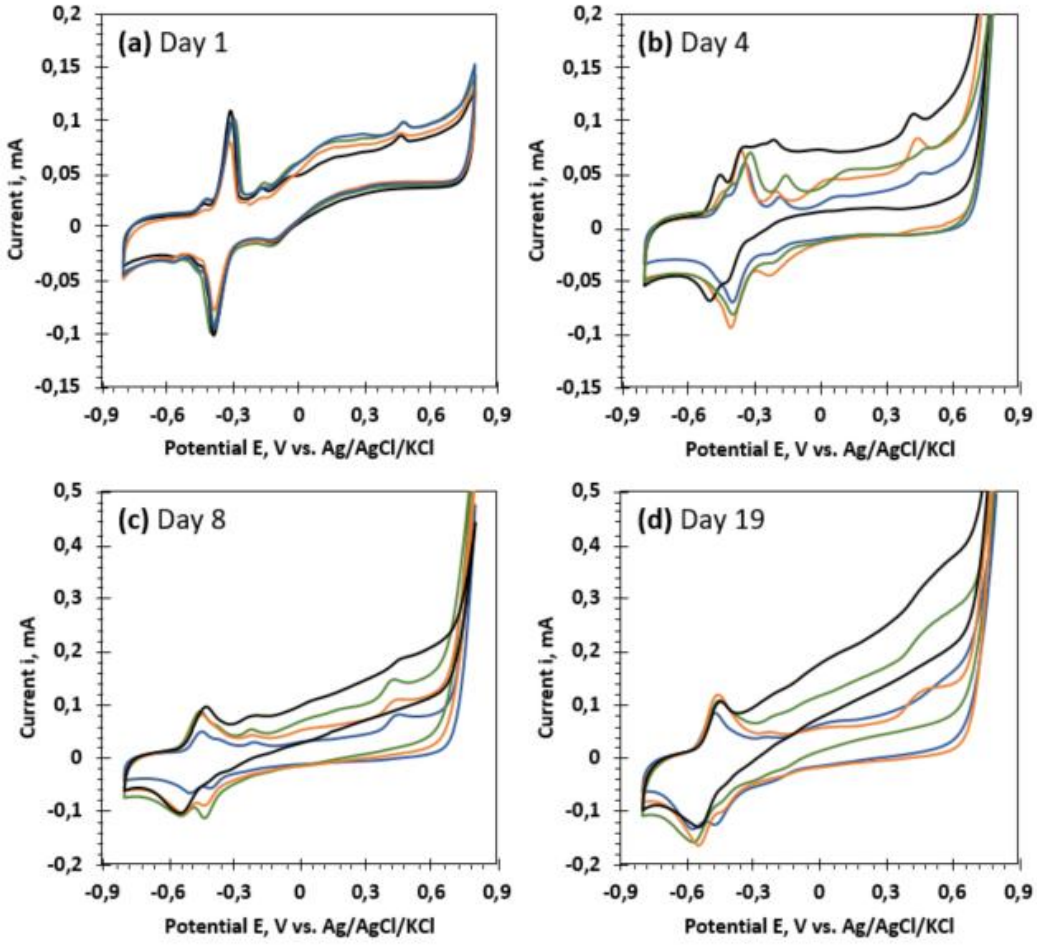
(a) Day 1
(b) Day 4
(c) Day 8
(d) Day 19
Current i, mA
Potential E, V vs. Ag/AgCl/KCl

FIGURE 4

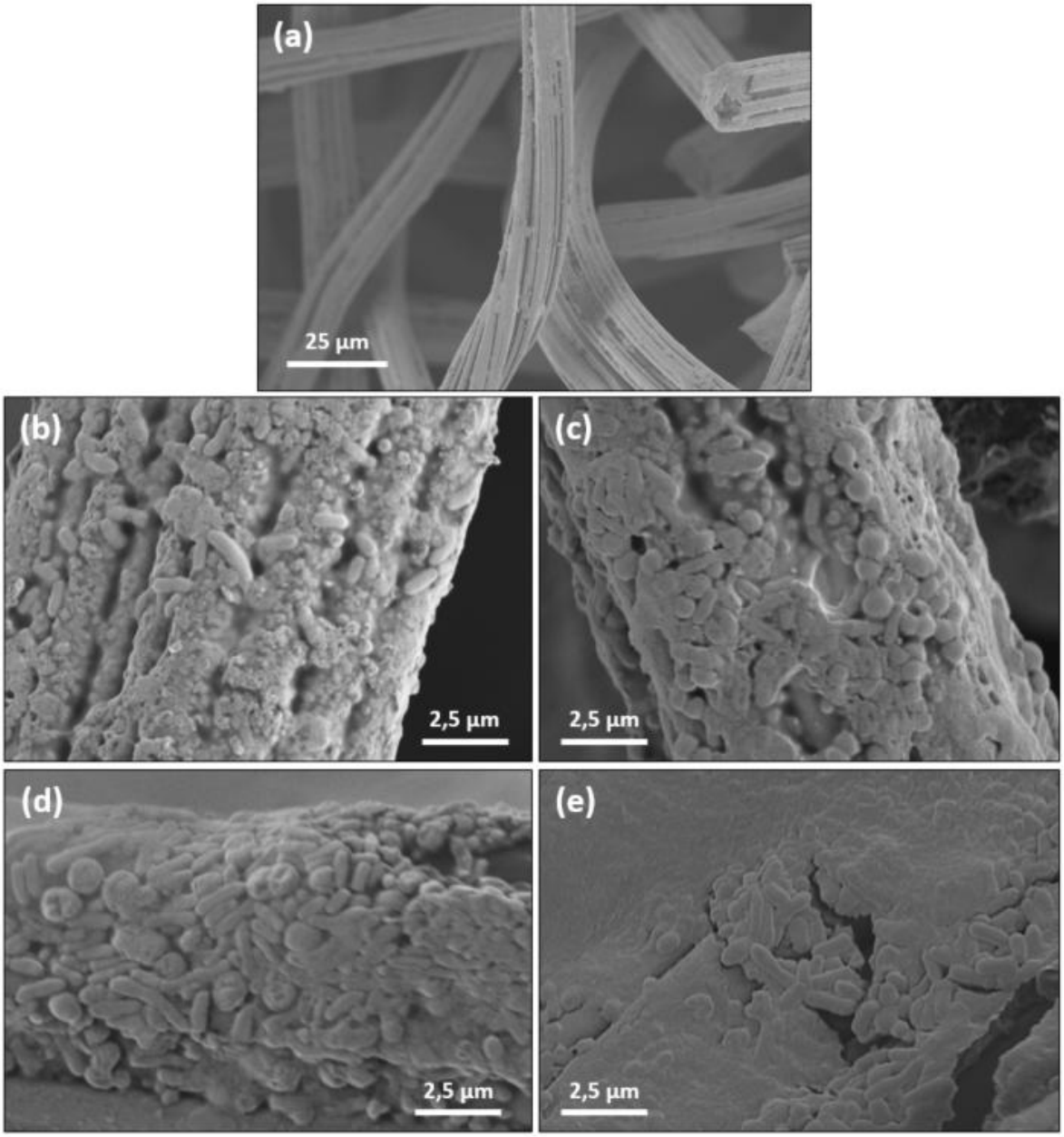

FIGURE 5

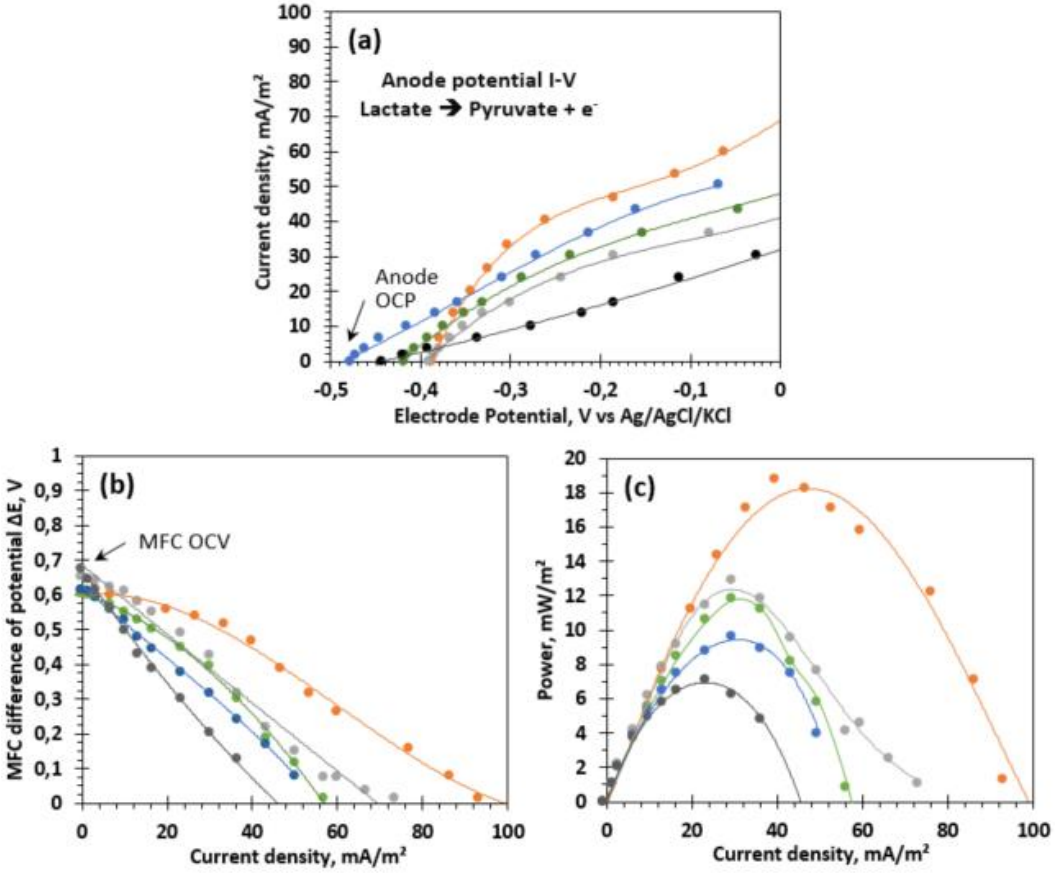
(a)
Anode potential I-V
Lactate → Pyruvate + e⁻
Anode OCP
Current density, mA/m²
Electrode Potential, V vs Ag/AgCl/KCl
(b)
MFC OCV
MFC difference of potential ΔE, V
Current density, mA/m²
(c)
Power, mW/m²
Current density, mA/m²

FIGURE 6

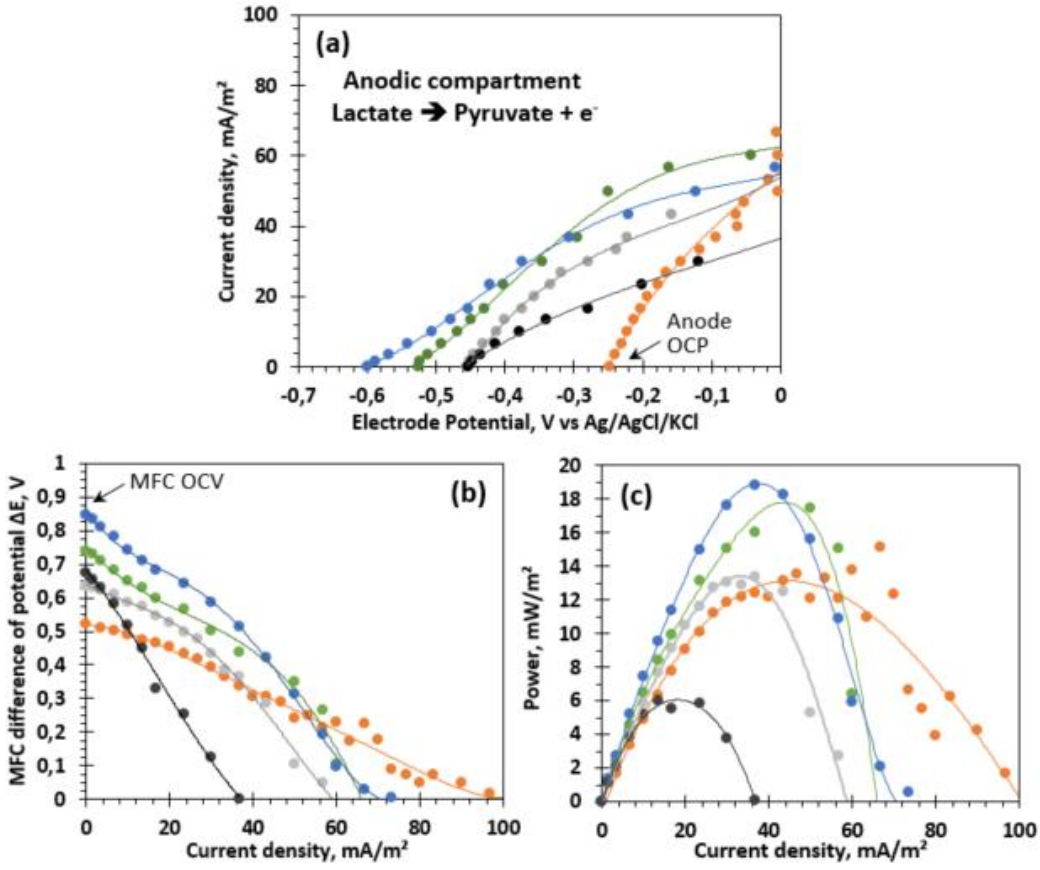
(a)
Anodic compartment
Lactate → Pyruvate + e⁻
Current density, mA/m²
Electrode Potential, V vs Ag/AgCl/KCl
Anode OCP
(b)
MFC OCV
MFC difference of potential ΔE, V
Current density, mA/m²
(c)
Power, mW/m²
Current density, mA/m²

FIGURE 7

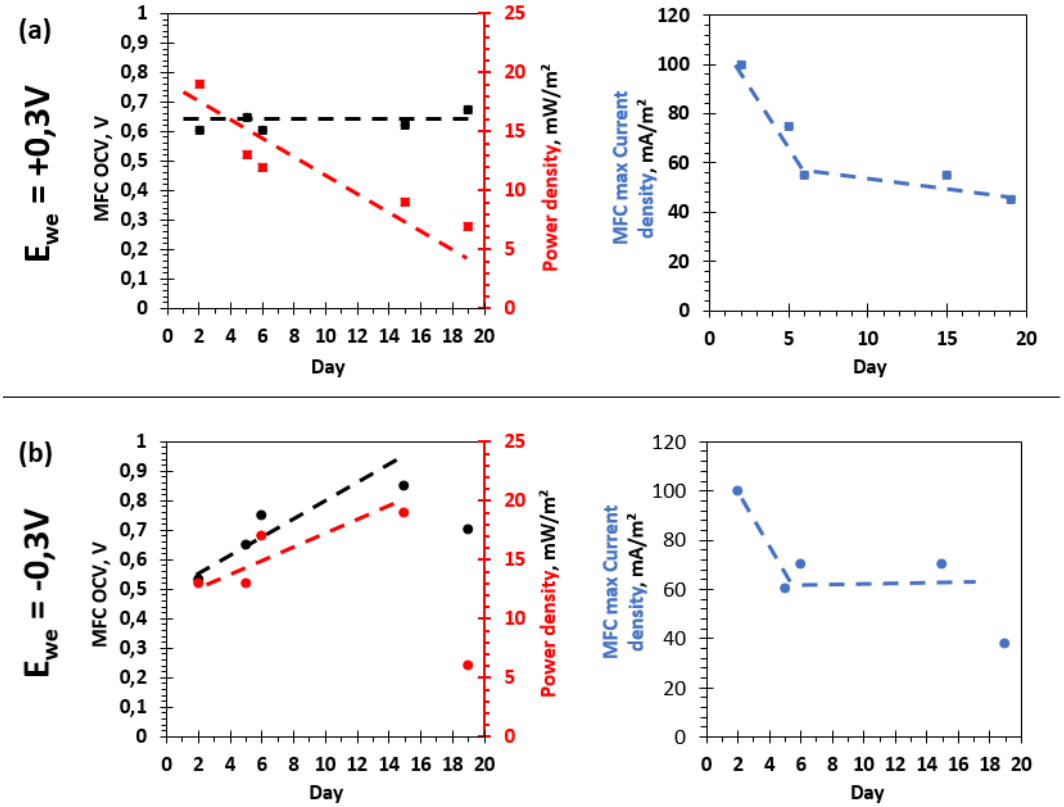

FIGURE 8